ACS OMEGA

http://pubs.acs.org/journal/acsodf

Article

Al_2O_3 Dispersion-Induced Micropapillae in an Epoxy Composite Coating and Implications in Thermal Conductivity

Zihe Pan,* Yanhong Liu, Fei Wang, Guangjun Lu, Fengling Yang, and Fangqin Cheng*

Cite This: *ACS Omega* 2021, 6, 17870−17879

Read Online

ACCESS | Metrics & More | Article Recommendations | Supporting Information

ABSTRACT: Al_2O_3 particles with different sizes were dispersed into an epoxy precursor to improve the thermal conductivity (TC) of the epoxy coating. Al_2O_3 particles tend to aggregate in epoxy, and the aggregation becomes more apparent (formation of micropapillae when the particle size is larger than 1 μm) with the increase of particle size. The calculated fast aggregation rates of various-size Al_2O_3 particles in epoxy showed that the fast aggregation rate increased to a maximum rate of 6.37×10^{-20} $m^3 \cdot s^{-1}$ at a particle size of 200 nm and then decreased to a plateau value with the increase of particle size. The high fast aggregation rate caused the aggregation and the formation of nano- and micropapillae, causing the heterogeneous distribution of Al_2O_3 particles. These micropapillae were separated by epoxy, which made formation of continuous pathways fail, causing the reduction of TC and heterogeneous heat distribution. The highest thermal conductivity of 2.52 W/m·K and uniform heat distribution were observed at the optimum filler size of 30 nm. The research findings provide the knowledge of optimizing particle size on constructing a thermally conductive polymer composite.

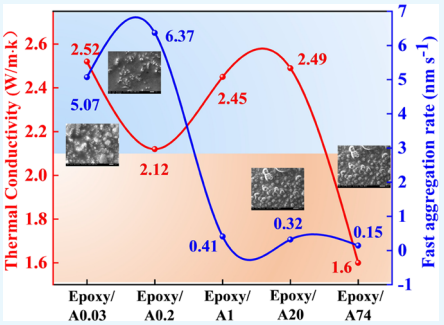

1. INTRODUCTION

Polymer composites (PCs) with certain thermal conductivity have been extensively utilized in miniaturization, high-power density, and high-performance electronic devices (flexible electronic skins,[1] plastic packaging,[2] batteries[3,4]) attributed to their significant advantages of light weight, ease of processing, low cost, high chemical/thermal stability, etc.[5−7] The high-power density devices might generate a huge amount of heat during operation, which needs to be timely eliminated.[8−10] Nevertheless, the comparatively low TC of PCs fails to quickly dissipate the generated heat, which causes the thermal failure or even the explosion of the devices.[11,12] As a consequence, there is an increasing demand for improving the thermal conductivity of PCs to meet the practical applications.[13−15]

PCs that are thermally conductive rely on the formation of conductive pathways, and the TC increases linearly with the increasing number of continuous conductive networks.[16] There are many factors affecting the formation of thermally conductive pathways, e.g., particle size, filler morphology, and interfacial compatibility between the fillers and polymer matrix.[6,17−20] The size of fillers plays a critical role in the formation of thermally conductive networks, e.g.,. nanosize fillers with extremely large surface areas are more favorable than microparticles for constructing a conduction path.[21] However, the high surface energy of nanofillers leads to aggregation and formation of thermal conduction barriers.[22] Recently, particle packing theory has been reported to construct consecutive thermal conductive pathways through bridging the lager particles with nanofillers to form closely compacted continuous networks.[23] Mao et al.[24] studied the particle size effects on thermal conductivity, showing that increasing the content of smaller particles resulted in higher thermal conductivity. Increasing the aspect ratio of thermally conductive fillers from sphere particles to wires,[25−27] pellets,[28,29] and sheets[30,31] is broadly utilized because of the ease of forming connection networks, e.g., the branched Al_2O_3 overlapped in phenolic resin to form conductive pathways, resulting in high TC.[32] Nevertheless, the dominant factor for the formation of conductive networks for thermally conductive fillers is their dispersion in the polymer matrix. The poor dispersion of fillers in polymers causes serious aggregations; thus, the thermally conductive fillers are separated by the polymer matrix, disallowing construction of continuous networks.[33,34]

The difficulty of uniformly dispersing the fillers in polymers is ascribed to the numerous formed interfaces between the fillers and polymers.[35] Thermally conductive fillers are first wetted by polymers and then dispersed in the polymer matrix, which might cause the formation of numerous thermal barriers prohibiting heat transformation.[36−39] He et al.[40] improved the TC of nano-Al_2O_3-based PCs from 0.23 to 0.26 W/m·K via the

Received: March 10, 2021
Accepted: June 25, 2021
Published: July 8, 2021

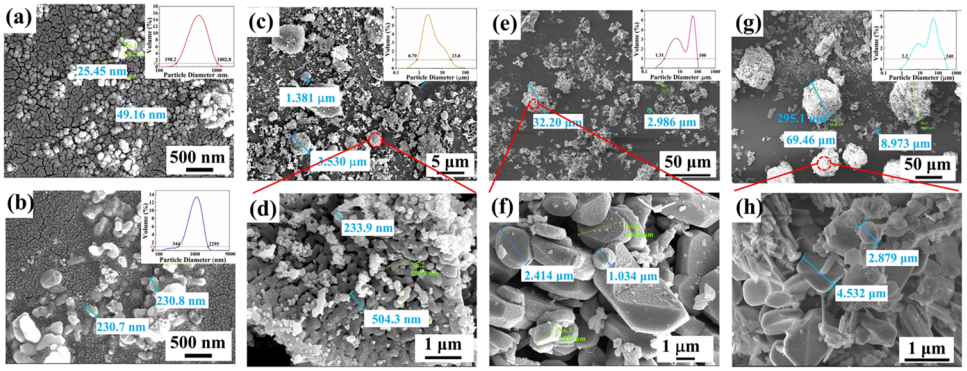

Figure 1. Surface morphology of Al_2O_3 particles with varied size: (a) A0.03, (b) A0.2, (c) A1, (e) A20, and (g) A74; (d) high-resolution SEM analysis of Al_2O_3 particles in (c); (f) high-resolution SEM analysis of Al_2O_3 particles in (e); (h) high-resolution SEM analysis of Al_2O_3 particles in (g).

modification of nano-Al_2O_3 with vinyl trimethoxysilane (VTMS).

Yang et al.[41] modified boron nitride (BN) platelets with poly(dopamine) (PDA) and γ-methacryloxypropyl trimethoxysilane (KH570) to lower down the interfacial thermal resistance of the filler-rubber, which enhanced the dispersion of BN, and the TC was improved from 0.26 to 0.39 W/m·K. Ralphs et al.[36] reported that the TC of the composite with less dispersion and more filler aggregations was larger than the TC of the composite with good dispersion due to the formed polydispersion. Though the TC was improved from 1.5 to 9.7 W/m·K with less dispersion, the filler aggregation might cause the nonuniform heat conduction and the failure of the PCs after long-term thermal operation. Consequently, the relationship between the particle size and dispersion with thermal conductivity is worth investigating to reveal the role of thermally conductive filler dispersion in obtaining highly thermally conductive homogeneous PCs.

In this study, we reported the dispersion of differently sized Al_2O_3 particles ranging from several nanometers to 100 μm in epoxy composites and the implications on thermal conductivity. The dispersion behaviors of Al_2O_3 particles with different sizes on the surface structure, the roughness of the epoxy-Al_2O_3 composite coatings, and the connections between Al_2O_3 particles were investigated. Furthermore, the wetting behavior of epoxy with the differently sized Al_2O_3 particles was also investigated to demonstrate the effective interactions between Al_2O_3 particles after wetting by epoxy, which can illustrate the possible thermally conductive pathway formation. The correlation between the dispersion of the differently sized Al_2O_3 particles with the thermal conduction performances was established. The research findings showed that there is an optimum particle size for enhancing the TC of epoxy composite coatings. Results showed that the aggregation of Al_2O_3 particles becomes more apparent with the increment of particle size. Though the microsized Al_2O_3 particle-filled epoxy coating showed similar thermal conductivity to nanosized Al_2O_3 particle-filled coatings, the significant aggregation of Al_2O_3 fillers caused the heterogeneous structure and thermal conductivity.

2. RESULTS AND DISCUSSIONS

The morphology and particle size of fillers are regarded as two important factors for the construction of thermally conductive pathways. As shown in Figure 1a, A0.03 particles are sphere-like and the measured size of particles ranged from 25 to around 45 nm with a relatively narrow size distribution (Figure 1a, inset image). Similarly, A0.2 particles are sphere-like (Figure 1b) with the measured size ranging from 198 to 1000 nm (Figure 1b, inset image). Unlike Al_2O_3 nanoparticles, the overall morphology of microsized Al_2O_3 is sphere-like (Figure 1c,e,g), while each of the spherical particles was composed of many agglomerated Al_2O_3 particles with different morphologies (Figure 1d,f,h). The aggregation of these smaller Al_2O_3 particles were further investigated by performing FTIR that showed that there are only reflection peaks of Al_2O_3, indicating the physical aggregations (Figure S1). The measured particle size ranges from 0.79 to 23.8 μm (Figure 1c, inset image), and some significant aggregations were detected in A1. Though the overall morphology of A20 (Figure 1d) and A74 (Figure 1f) is spherical, each particle is composed of smaller particles with an irregular morphology (Figure 1e,g). These smaller Al_2O_3 particles inside each sphere particle lead to the wide size distribution of A1, A20, and A74. Table 1 shows that the D_v (50) values of A1, A20, and A74 are 3.31, 8.63, and 67.2 μm, respectively, which corresponds well with the particle size in the SEM images in Figure 1.

Table 1. Particle Size Distribution of A1, A20, and A74 Particles

	1−3 μm Al_2O_3	20 μm Al_2O_3	74−149 μm Al_2O_3
D_v (10) (μm)	1.30	2.26	11.6
D_v (50) (μm)	3.31	8.63	67.2
D_v (90) (μm)	14.5	62.6	132

The surface morphology and surface profile after blending differently sized Al_2O_3 particles were explored to demonstrate the formation of conductive pathways in an epoxy precursor. As shown in Figure 2, the dispersion of Al_2O_3 in epoxy was investigated via characterizing the surface morphology of epoxy/Al_2O_3 composite coatings. A0.03 nanoparticles were dispersed well in epoxy and formed many oriented pathways (Figure 2a). Al_2O_3 nanoparticles occupied most of the surface area, and the clean epoxy between the oriented pathways was very limited (Figure 2a). However, a small amount of Al_2O_3 nanoparticles was observed on the epoxy coating surface when using A0.2 nanoparticles (Figure 2b); the formed conductive pathways were much fewer; and the orientations of the pathways were randomly distributed on the surface (Figure 2b). More continuous pathways were formed by using microscale A1 particles compared to epoxy/A0.2 (Figure 2c),

https://doi.org/10.1021/acsomega.1c01282
ACS Omega 2021, 6, 17870−17879

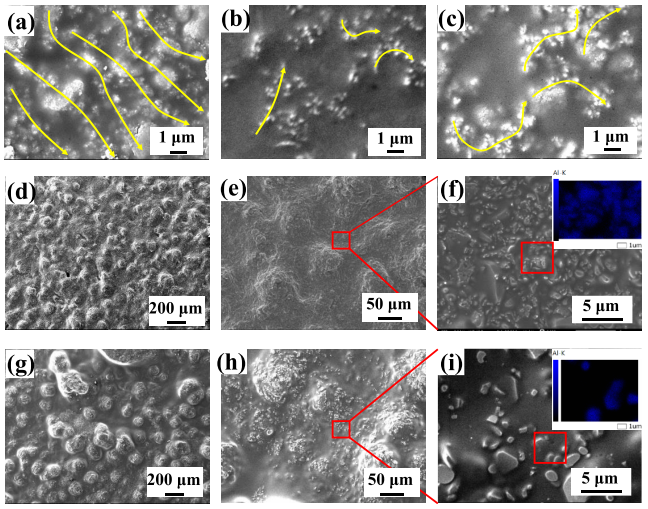

Figure 2. Surface morphology of epoxy/Al_2O_3 composite coatings. (a–c) Surface morphology of epoxy/A0.03, epoxy/A0.2, and epoxy/A1 composite coatings; (d) overall morphology of the epoxy/A20 composite coating; (e) high magnification of the epoxy/A20 composite coating; (f) surface morphology between the micropapillae and the EDS analysis of Al element distribution; (g) overall morphology of the epoxy/A74 composite coating; (h) high-magnification SEM image of spaces between micropapillae; (i) analysis of the distribution and formation of conductive pathways of Al_2O_3 in the area between micropapillae via SEM and EDS.

and there is a tendency of aggregation of Al_2O_3 particles (Figure 2c). Similarly, the microsized A1 particles are filled with epoxy, making the Al particles fail to connect (Figure 2c). Continuously increasing the particle size of Al_2O_3 caused more apparent aggregation. Many micropapillae are detected on the surface of epoxy coatings after incorporating A20 (Figure 2d), and the size of these micropapillae is around 20 μm (Figure 2d). These micropapillae are independent, which makes it difficult to form continuous pathways (Figure 2d, e). After looking into the space between these distributed micropapillae, a good many homogeneously dispersed smaller Al_2O_3 particles were found (Figure 2f) and these dispersed Al_2O_3 particles formed connected pathways (Figure 2f, inset EDS image). These homogeneously dispersed smaller Al_2O_3 particles might be due to the epoxy being wetted and filled into larger Al_2O_3 particles during the mixing process because the larger Al_2O_3 particles are composed of smaller particles and the formation is ascribed to the physical aggregation (Figure S1), which is easy to break during the mixing of Al_2O_3 particles and epoxy. Larger micropapillae are formed (~50 μm) when the size of Al_2O_3 particles increased to larger than 74 μm (Figure 2g). The dispersion of Al_2O_3 particles between micropapillae is investigated via SEM and EDS, showing that some smaller size Al_2O_3 particles (several micrometers) dispersed between the micropapillae (Figure 2h) and the dispersed Al_2O_3 particles were isolated without any connections (Figure 2i). The aggregation became more apparent with the increase of particles size and made it difficult to form connected pathways

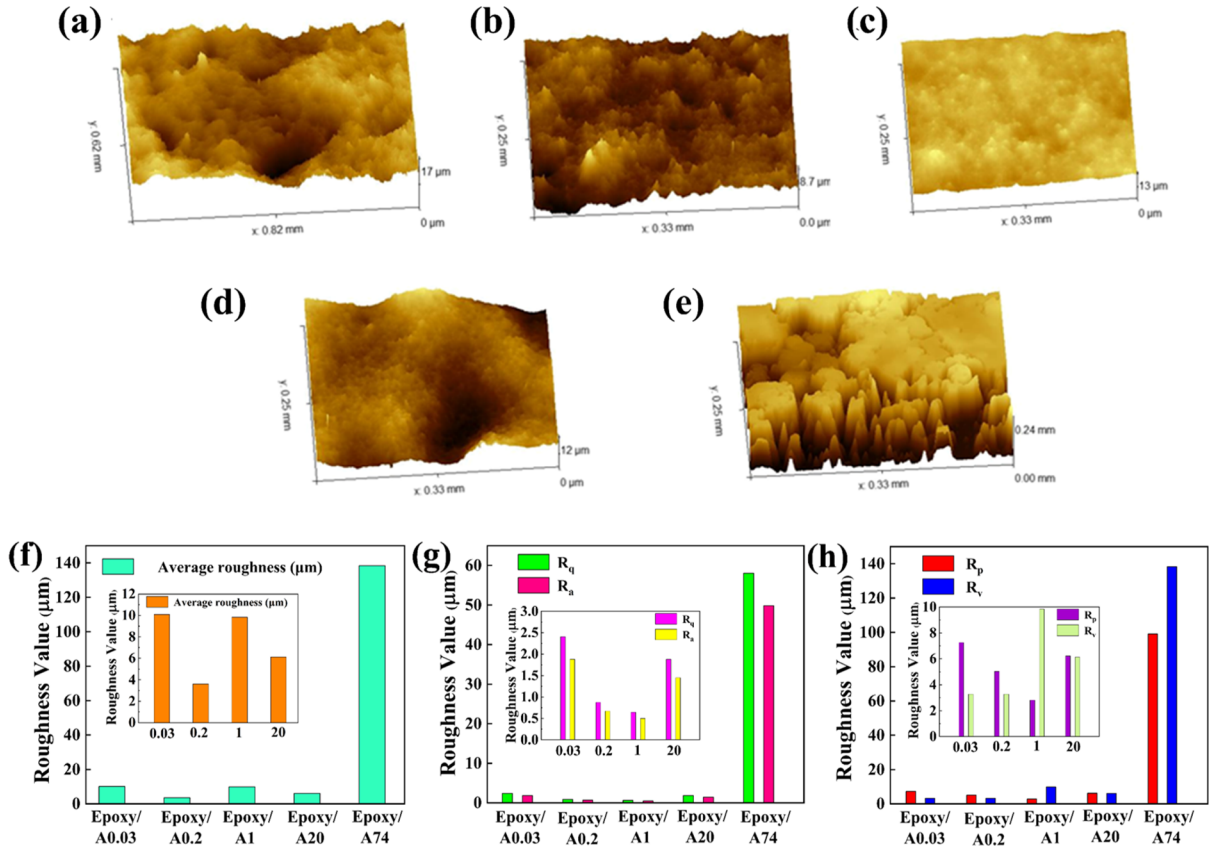

Figure 3. Surface profile of the composite coatings. (a) 3D surface profile of the epoxy/A0.03 composite coating; (b) 3D surface profile of the epoxy/A0.2 composite coating; (c) 3D surface profile of the epoxy/A1 composite coating; (d) 3D surface profile of the epoxy/A20 composite coating; (e) 3D surface profile of the epoxy/A74 composite coating; (f–h) average surface roughness, R_a and R_q, and R_p and R_v values of the five types of epoxy/Al_2O_3 composite coatings.

https://doi.org/10.1021/acsomega.1c01282
ACS Omega 2021, 6, 17870–17879

between each papilla, which might generate adverse effects on thermal conductivity.

To further investigate the effects of dispersed Al_2O_3 particles on the surface structure, an optical profilometer was applied to measure the surface profiles of the composite coatings (Figure 3). A large number of microgrooves and bumps are observed on composite coatings (Figure 3a–e). This result corresponded well with the surface microstructure of these composite coatings in Figure 2. The effects of particle size on the surface roughness are shown in Figure 4f–h, indicating

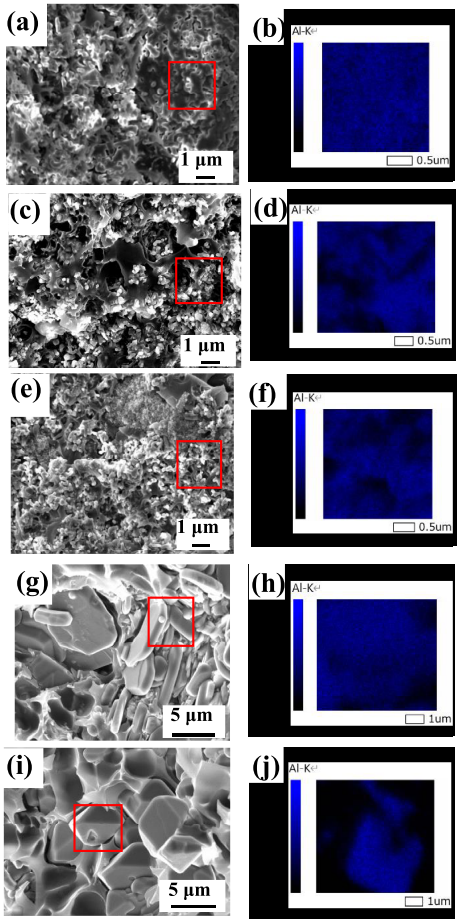

Figure 4. Cross-sectional analysis of the formation of conductive pathways via SEM and EDS of (a, b) epoxy/A0.03 (30 nm), (c, d) epoxy/A0.2 (200 nm), (e, f) epoxy/A1 (1–3 μm), (g, h) epoxy/A20 (20 μm), and (i, j) epoxy/A74 (74–149 μm) composite coatings.

that the surface roughness increased with the particle size except the epoxy/A0.2 composite coating. The average surface roughness of epoxy/A0.03 is larger than the surface roughness of epoxy/A0.2, A1, and A20 (Figure 3f). The surface height change of composite coatings is described by the arithmetic mean surface roughness (R_a) and root mean square roughness (R_q).[42] The R_a and R_q epoxy/A74 in Figure 4g (with R_a and R_q of 49.85 and 58.04 μm, respectively) are much higher than that of other composite coatings (in which R_a < 2 μm and R_q < 3 μm) (Figure 3g). Moreover, the maximum peak (R_p) of epoxy/A74 is 99.109 μm and the maximum peak-valley depth (R_v) is 138.28 μm. The average roughness of epoxy/A74 (138.28 μm) is also the largest in these specimens, which leads to the formation of "isolated islands" between the surface fillers (Figure 3h). With this structure, it is difficult to form effective heat flow networks.

Though the dispersion of Al_2O_3 particles on the surface morphology, surface profiles, and the formation of conductive pathways have been discussed, the dispersion of Al_2O_3 particles inside the epoxy is more vital for the formation of continuous pathways. The formed conductive networks in composite coatings were investigated by characterizing the cross section of epoxy/Al_2O_3 composite coatings via SEM and EDS. As shown in Figure 4a,b, Al_2O_3 nanoparticles dispersed uniformly in the epoxy/A0.03 composite coating and formed compacted connections. The EDS result of Al showed that uniformly dispersed Al_2O_3 nanoparticles were observed in the epoxy/A0.03 composite coating without aggregation, thereby forming numerous continuous connection pathways (Figure 4b). However, Al_2O_3 nanoparticles were scattered on the epoxy/A0.2 coating and were separated by epoxy (Figure 4c), as revealed by the EDS result of Al (Figure 4d). In addition, a larger surface area of the disconnected structures was observed (Figure 4d), indicating the poor dispersity of A0.2 nanoparticles in the epoxy precursor (Figure 4d) though small aggregations can be seen in the epoxy/A1 composite coating (which was filled with A1 microparticles) (Figure 4e,f). These well-dispersed Al_2O_3 microparticles contacted compactly, generating effective pathways (Figure 4f). As shown in Figure 4g,h, the epoxy precursor entered into the large Al_2O_3 nanoparticles (20 μm) and coated at the surface of the smaller Al_2O_3 nanoparticles, forming the barriers between Al_2O_3 nanoparticles. The finer Al_2O_3 partices in the larger Al_2O_3 particles were coated and separated by epoxy which failed to form connective pathways causing the formation of larger interfacial thermal resistance. (Figure 4i,j). The dispersion of Al_2O_3 particles can also be verified from the EDS elemental distribution (Figure S3), showing that there are significant Al and peaks in the epoxy/A0.03 coating while the intensity of C is quite low. However, with the increase of particle size, the intensity of Al decreased, while the intensity of C increased (Figure S3). Figure S3e shows that one Al_2O_3 particle was surrounded by C and prevented from connecting with other Al_2O_3 particles, leading to less pathway formation.

The dispersion behavior of the filler is of great significance to the formation of the heat conduction path. In order to further explore the distribution of Al_2O_3 with different particle sizes in the composite coating, the 3D structure and 2D slices using the X-ray imager (XRT) were used to study the distribution of Al_2O_3 in the epoxy/Al_2O_3 composite coating (Figure 5). The figure shows the 2D and 3D information of the epoxy/Al_2O_3 composite coatings prepared with different particle sizes of Al_2O_3. On the same scale, different colors represent different particle sizes. The composite coatings prepared using different particle sizes of Al_2O_3 show different colors. Due to the large amount of filler filling, the 3D graph shows that the filling of the filler is denser. It can be seen from the figure that the agglomerated particles of nanofillers are smaller, while the agglomerated particles of micrometer fillers are larger and their dispersibility is poor. It can be seen from the 3D and 2D slices in Figure 5a–c that the epoxy/0.3, epoxy/0.02 and epoxy/A1 composite coatings have better dispersibility. On the other hand, the agglomeration of particles in the composite coating of epoxy/A20 and epoxy/A74 is larger and the dispersion is worse, but the agglomerated particles of epoxy/A20 are smaller than those of epoxy/A74 (Figure 5d,e). From the 3D distribution of Figure 5d,e and the

https://doi.org/10.1021/acsomega.1c01282
ACS Omega 2021, 6, 17870–17879

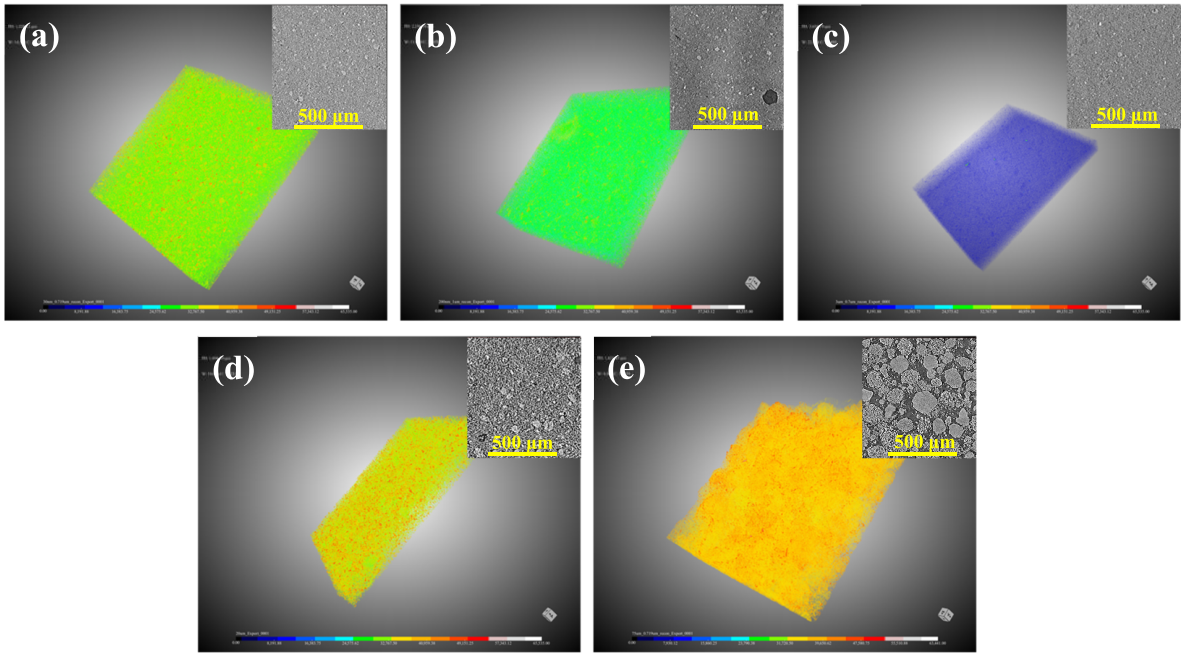

Figure 5. X-ray tomography data of Al_2O_3 with different particle sizes in the composite coating. (a) 3D image and 2D image of the epoxy/A0.03 composite coating; (b) 3D image and 2D image of the epoxy/A0.2 composite coating; (c) 3D image and 2D image of the epoxy/A1 composite coating; (d) 3D image and 2D image of the epoxy/A20 composite coating; (e) 3D image and 2D image of the epoxy/A74 composite coating.

slice diagram at the top right, both large and small particles in the epoxy/A20 composite coating and the small particles connected the aggregations, resulting in a denser internal structure and conductive pathways, while the particle agglomeration of epoxy/A74 is very large, causing the separation of aggregations and the discontinuous Al_2O_3 pathways. As shown in 2D slices (Figure 5e), the large agglomerated particles are filled with a large amount of epoxy resin, so forming an effective heat conduction path is difficult.

One of the critical points of the formation of conductive pathways is the complete wetting of fillers by the matrix polymer, and therefore effective interactions between the fillers are generated to enhance the TC of PCs.[43] Consequently, the wetting behaviors of epoxy on differently sized Al_2O_3 particles were investigated. To explain the aggregation of differently sized Al_2O_3 particles, the fast aggregation rate was used and calculated through the following equation:[44,45]

$$(K_{11})_{\text{fast}} = \frac{8K_BT}{3\eta} \quad (1)$$

where K_B is the Boltzmann constant, T is the absolute temperature, and η is the viscosity of the polymer precursor (Figure S4). The fast aggregation rate of differently sized Al_2O_3 particles was plotted as a function of particle size (Figure 6a), showing that the fast aggregation rate increased to the maximum value of 6.37×10^{-20} $m^3 \cdot s^{-1}$ with the increasing particle size and then decreased to 0.15×10^{-20} $m^3 \cdot s^{-1}$. This behavior illustrated that Al_2O_3 with the particle size of 200 nm was quickly wetted and separated by epoxy, causing the formation of less conductive pathways. The fast aggregation rate of microsized Al_2O_3 particles is much smaller than that of nanosized Al_2O_3 particles, leading to the slow wetting of epoxy on microsized Al_2O_3 particles, which promoted the formation of micropapillae.

As shown in Figure 6a, the microsized Al_2O_3 samples (A1: 1−3 μm, A20: 20 μm, and A74: 74−149 μm) are wetted faster

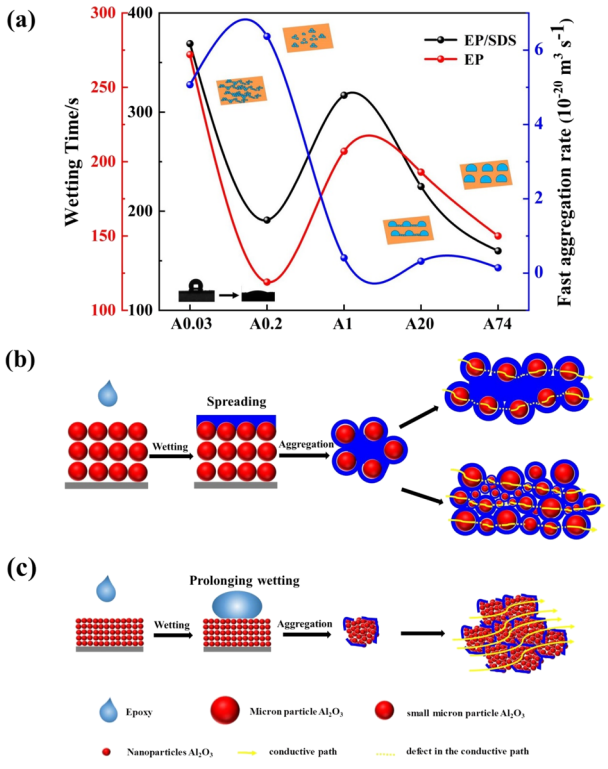

Figure 6. (a) Wetting of epoxy resin on differently sized Al_2O_3 particles; proposed wetting mechanism of epoxy on (b) microsized and (c) nanosized Al_2O_3 particles.

than the nanosized Al_2O_3 (A0.03: 30 nm). The only exception is the Al_2O_3 with a particle size of 200 nm where the particles were completely wetted by epoxy within 130 s (Figure 6a). A similar trend was also found when using the original epoxy to wet the differently sized Al_2O_3 (Figure 6a). Therefore, we speculate that in the process of preparing the composite

https://doi.org/10.1021/acsomega.1c01282
ACS Omega 2021, 6, 17870−17879

coating, the microsized Al_2O_3 particles were first wetted and wrapped by epoxy resin (Figure 6b) and then the agglomerates are formed,[46] which can be verified by the SEM image in Figure 5. This phenomenon is more apparent with utilizing larger particles (A20 and A74 particles). Because the large A20 and A74 particles are composed of many small particles, the epoxy wetted these small particles and separated them from connection. A similar phenomenon was also found in the original epoxy (high viscosity) where the epoxy filled the internal gaps of microsized Al_2O_3 particles and caused the limited continuous pathway formation (Figure S5). As a consequence, the conductive pathways are much less in epoxy/A20 and epoxy/A74 composite coatings. On the contrary, nanoscale Al_2O_3 particles first formed interactions with each other and then were wetted by epoxy resin (Figure 6c). However, the TC of composites filled with nanoparticles of different sizes is varied, which might be because smaller particles always have a larger specific surface area, resulting in the larger agglomeration capacity of A0.03 particles than A0.2 particles, denser composites, and more thermal conductivity pathways. A brief conclusion was drawn in that there is an optimum particle size for the TC of PCs and TC is correlated with the wetting and dispersion of the particles in polymers. Though microsized particles might induce high thermal conductivity in polymers, the significant aggregation leads to the heterogeneous thermal conductivity, which affects the long-term stability of thermally conductive coatings.

The thermal conduction performances of epoxy/Al_2O_3 (70 wt %) composite coatings incorporated with different particle sizes of Al_2O_3 were investigated in terms of TC and thermal diffusivity (TD). The TC and TD of epoxy/Al_2O_3 composite coatings are higher than 1.50 W/m·K and 0.80 mm^2/s, respectively, while the TC of the original epoxy resin is 0.2 W/m·K, indicating the effectiveness of Al_2O_3 particles on improving the TC of epoxy (Figure 7). The TCs of epoxy/A0.03 (Al_2O_3: 30 nm), epoxy/A1 (Al_2O_3: 1−3 μm), and epoxy/A20 (Al_2O_3: 20 μm) are similar with values of 2.52, 2.45, and 2.49 W/m·K, while their TDs are different with values of 1.66, 1.34, and 1.56 mm^2/s, respectively. The TC of epoxy coating dropped to 2.12 when incorporated with 200 nm Al_2O_3 particles (epoxy/A0.2), and the TC reduced to the lowest value after the epoxy was filled with 74 μm Al_2O_3 particles (epoxy/A74) (Figure 7). The same tendency was found for their TD value. The above results demonstrated that TC is closely related to the filler size. In this study, The TC of the epoxy coating is larger than 2.0 W/m·K when the size of the Al_2O_3 filler is smaller than 20 μm. With the continuous increase of the filler size to larger than 74 μm, the thermal conductivity dropped the smallest. Though the TCs of epoxy/A0.03 and epoxy/A20 coatings are similar, the TD of epoxy/A20 is smaller than that of epoxy/A0.03, showing that the optimum filler size is 30 nm.

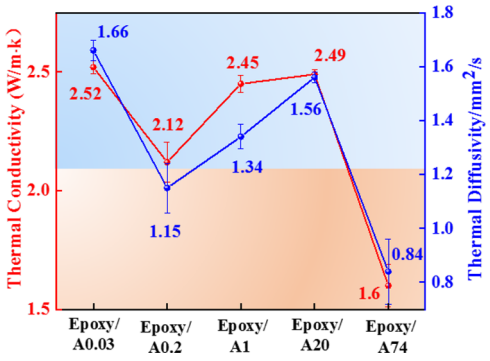

Figure 7. Thermal conductivity and thermal diffusivity of epoxy composite coatings with different particle sizes of Al_2O_3 with the filling concentration of 70 wt %.

Since the thermal conductivities of epoxy/A0.03, epoxy/A1, and epoxy/A20 composite coatings are similar, further characterization was performed to compare the thermal conductivity of these composite coatings through infrared imaging devices. Figure 8a is the control experiment on a hot plate. Figure 8b is the heat distribution of the epoxy/A0.03 composite coating and shows that the whole surface area is bright, indicating the homogeneous distribution of A0.03 nanoparticles in epoxy. However, the heat distribution of the epoxy/A0.2 composite coating is heterogeneous; the blue circle is dim, while the green circle is brighter than other parts (Figure 8c) and the whole area is not as bright as in Figure 8b, indicating the differences in thermal conductivity. This phenomenon is more evident in the epoxy/A1 composite coating because its thermal conductivity is similar to that of the epoxy/A0.03 composite coating (Figure 8d). There is only a small part of the epoxy/A1 composite coating (circled area) that is bright, while most of the area is dim, showing the heterogeneous distribution of particles and aggregations of the particles (Figure 8d). There are many dark spots observed on the epoxy/A74 composite coating, while other pats are bright, which corresponds well with the surface structure of the epoxy/A74 composite coating (many micropapillae distributed on the surface) (Figure 8e). The surface of the epoxy/A74 composite coating is much dimmer in all of the five samples, indicating the lowest thermal conductivity (Figure 8f). The digital images of the heat distribution of the five samples further confirmed that the TC is closely related to the dispersion of particles in epoxy and the aggregation. The result verifies that the TCs of epoxy/A0.03, epoxy/A1, and epoxy/A20 composite coatings are similar and their heat distribution varied significantly due to the distribution and aggregation of different size particles. A brief conclusion can be drawn in that the epoxy filled with 30 nm (A0.03) showed the best thermal conduction performance.

3. EXPERIMENTAL SECTION

3.1. Materials. Bisphenol A epoxy resin (DER331, Dow Chemical Company) and 593 curing agents were purchased from Shanghai Aotun Chemical Technology Co., Ltd. The thermally conductive filler is alumina (Al_2O_3) with a density of 3.97 g/cm^3. Al_2O_3 samples with particle sizes of 30 and 200 nm (purity, 99.99% metals basis) were provided by Shanghai Macklin Biochemical Co, Ltd. α Phase Al_2O_3 with a particle size of 1−3 μm (purity, ≥99.99% metals basis) was provided by Shanghai Piper Biotechnology Co., Ltd. Al_2O_3 samples with particle sizes of 20 and 74−149 μm (purity, 99.9% metals basis) were supplied by Innochem, Beijing. Sodium dodecyl sulfate (SDS) (purity AR, ≥92.5%) was supplied by Shanghai Macklin Biochemical Co, Ltd. Isopropanol (purity AR, ≥99.5%) was provided by Shanghai Macklin Biochemical Co, Ltd.

3.2. Sample Preparation. A series of epoxy-Al_2O_3 composite coatings were prepared with adding different amounts of differently sized Al_2O_3 particles (Table 2). The procedures of fabrication of epoxy-Al_2O_3 composite coatings

https://doi.org/10.1021/acsomega.1c01282
ACS Omega 2021, 6, 17870−17879

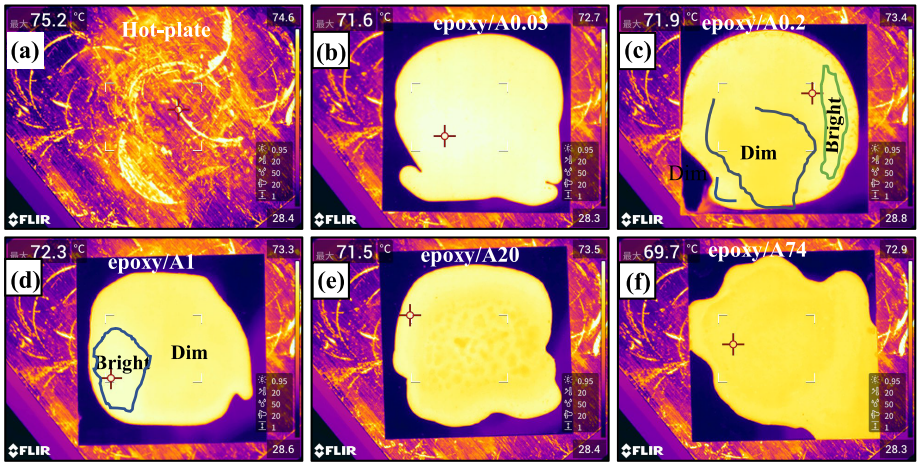

Figure 8. Heat distribution of different epoxy/Al_2O_3 composite coatings: (a) control group of the hot plate and (b–f) heat distribution of epoxy/A0.03, epoxy/A0.2, epoxy/A1, epoxy/A20, and epoxy/A74 composite coatings, respectively.

Table 2. List of the Fabricated Epoxy/Al_2O_3 Composite Coatings and the Particle Size Information of Utilized Al_2O_3 Particles

	Al_2O_3	loading	isopropanol
epoxy/A0.03	30 nm	70 wt %	2.6 mL/g
epoxy/A0.2	200 nm	70 wt %	2.4 mL/g
epoxy/A1	1–3 μm	70 wt %	2.2 mL/g
epoxy/A20	20 μm	70 wt %	2.0 mL/g
epoxy/A74	74–149 μm	70 wt %	1.8 mL/g

are illustrated in Figure 9. First, a certain amount of sodium dodecyl sulfate (SDS) was dissolved into isopropanol. Then, a low-power ultrasonic bath (SB-5200DTDN, 200 W, Ningbo Xinzhi Biotechnology Company, China) was used to sonicate the solution for 15 min. The SDS concentration in isopropanol is 0.06 mol/L.[47] SDS was used to enhance the dispersion and reduce the aggregation of Al_2O_3 particles.[48,49] After that, a certain amount of Al_2O_3 particles was added into the SDS solution to prepare a homogeneously dispersed Al_2O_3 solution (SDS-Al_2O_3). SDS is 4.5 wt % of Al_2O_3. Al_2O_3 was added to

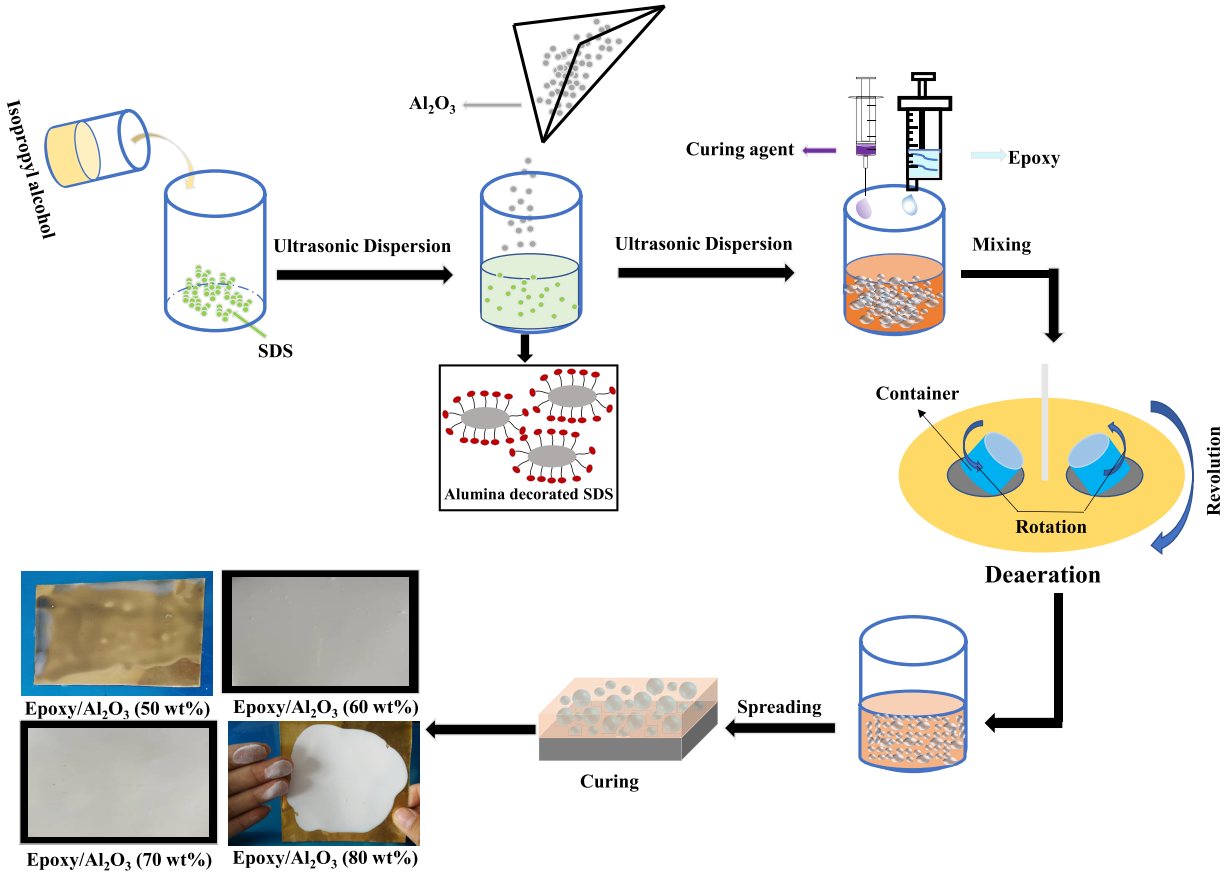

Figure 9. Schematic illustration of the fabrication of epoxy-Al_2O_3 composite coatings.

https://doi.org/10.1021/acsomega.1c01282
ACS Omega 2021, 6, 17870–17879

the dispersion of SDS and then treated with low-power ultrasound for 30 min. In order to remove unbonded SDS, it was washed with isopropanol, centrifuged (Sigma 3 K15, Sigma Company, German) at 8000 rpm for 10 min to remove the supernatant, and then dried in a vacuum oven at 60 °C to obtain SDS-Al_2O_3 powder.[47] FTIR was applied to verify SDS-functionalized Al_2O_3 (Figure S1). Epoxy and the curing agent were added into the SDS-Al_2O_3 solution and were transferred to a mixer (HM600A, Shenzhen Ha Sai Technology Co., Ltd.) to mix well Al_2O_3 and epoxy. The air bubbles and the solvent were removed completely during mixing (Figure 9). Then, the obtained well-dispersed epoxy-Al_2O_3 composite precursor was casted onto a flat aluminum sheet and cured under room temperature at 25 °C for 24 h. The average thickness of the epoxy-Al_2O_3 composite coating was 0.2 mm ± 0.029 mm.

A series of epoxy-Al_2O_3 composite coatings were prepared with the Al_2O_3 weight ratio ranging from 50 to 80 wt % (Figure 9). However, the coating and the Al_2O_3 particles are easily peeled off from the sheet when the content of Al_2O_3 is 80 wt %, while the as-prepared composite coatings are either transparent (50 wt % loading of Al_2O_3) or with low thermal conductivity (60 wt % loading of Al_2O_3). Therefore, the composite coating with a loading of 70 wt % was selected as the model to illustrate the dispersion of different Al_2O_3 particles in epoxy, and the sample information is listed in Table 2.

3.3. Characterization. The particle size distribution of Al_2O_3 of 1−3 (A1), 20 (A20), and 74 μm (A74) was analyzed by a Marvin particle size meter (Mastersizer 3000, Malvern Instruments Co., Ltd., UK). The surface chemistry of different sizes of Al_2O_3 particles after surface modification was analyzed by Fourier transform infrared spectrometry (FTIR, PerkinElmer 2000, USA). The surface morphologies of the Al_2O_3 and epoxy-Al_2O_3 composites were characterized by scanning emission electron microscopy (SEM, JSM-IT500HR/LV, Tokyo, Japan) at an accelerating voltage of 10 kV. A planetary defoaming mixer (HM600A, Shenzhen Ha Sai Technology Co., Ltd.) was used to mix the composite homogeneously. The surface profiles of the as-prepared composite coatings were characterized by an optical profilometer (MFP-D WLI 3D surface profilometer, Rtec Instruments Inc., USA). The wetting behavior of epoxy resin on differently sized Al_2O_3 particles was measured via the sessile drop method (KrussDSA25, Germany) by placing 10 μL of epoxy resin onto Al_2O_3 particles. At least three samples were fabricated, and each sample was measured three times to obtain the average contact angle. The thermal conductivity of the composites was determined by a laser flash thermal conductivity instrument (LFA 447 instrument, Germany) at 25 °C, which is calculated from the following equation:[50]

$$\lambda = \alpha \times \rho \times C_P \quad (2)$$

where λ is the thermal conductivity (W/m·K), α is the thermal diffusion coefficient (m^2/s), ρ is the composite density (kg/m^3), and C_p is the specific heat capacity (J/kg·K). 0.2 mm-thick flat sheet samples were cut into circles with a diameter of 25.4 mm using a hollow punch. Before testing, the sample was spray-coated with carbon black to prevent the laser beam from penetrating the sample. From the laser flash thermal conductivity instrument (LFA 447), the in-plane thermal diffusion coefficient was measured. Each group sample was measured three times to obtain the average thermal diffusion coefficient. Specific heat capacity was measured using a specific heat tester (DSC 200F3, Gallic instruments Inc., Germany). The density of the sample was calculated through the Archimedes immersion principle. The XRT (Xradia 610 Versa, Germany) submicrometer resolution was used to measure the 3D distribution of Al_2O_3 with different particle sizes in the epoxy/Al_2O_3 composite coating, as well as the 2D slice information of the composite coating. The heat distribution of these composite coatings was measured by an infrared thermal imager (E85 24°, FLIR, USA). First, the temperature of the hot plate was raised to 80 °C, and then the sample was placed on a hot plate after the temperature of the hot plate was stable. After 3 min, the surface of the sample was photographed with a thermal imager. After that, each specimen was placed on the hot plate and heated for 3 min before taking the image.

4. CONCLUSIONS

In summary, the dispersion of differently sized Al_2O_3 particles in an epoxy precursor and its effects on the thermal conduction performances have been studied. Results showed that A0.03 nanoparticles (30 nm) homogeneously dispersed without significant aggregation in epoxy forming oriented straight-line conductive pathways resulting in the highest thermal conductivity. However, the incorporation of A0.2 nanoparticles (200 nm) reduced the thermal conductivity because A0.2 nanoparticles were quickly wetted by the epoxy precursor, leading to the separation of Al_2O_3 particles by epoxy, which failed to form effective and enough conductive pathways. Though increasing the particle size of Al_2O_3 in epoxy results in the increment of thermal conductivity, the aggregations became more significant. A good many micropapillae were formed and homogeneously distributed on the epoxy composite coatings leading to the discontinuous pathways. The heat distribution of as-prepared composite coatings showed that the epoxy/A0.03 coating is the brightest, while epoxy/A74 coating is the dimmest one corresponding well with the thermal conductivity. This research illustrated the optimum particle size of Al_2O_3 to construct epoxy composite coatings with high and homogeneous thermal conductivity.

■ ASSOCIATED CONTENT

Supporting Information

The Supporting Information is available free of charge at https://pubs.acs.org/doi/10.1021/acsomega.1c01282.

Chemical properties of Al_2O_3 with different particle sizes, verification of the interaction between Al_2O_3-SDS and epoxy, dispersion state of Al_2O_3 in epoxy resin, rheological performance test of composite coatings prepared by Al_2O_3 with different particle sizes, analysis of the wetting behavior of epoxy resin to Al_2O_3, and verification of the interaction between Al_2O_3 and SDS (PDF)

■ AUTHOR INFORMATION

Corresponding Authors

Zihe Pan − *Institute of Resources and Environmental Engineering & Shanxi Collaborative Innovation Center of High Value-Added Utilization of Coal-Related Wastes, Shanxi University, Taiyuan, Shanxi 030006, China;* orcid.org/0000-0002-8323-0199; Email: panzh@sxu.edu.cn

https://doi.org/10.1021/acsomega.1c01282
ACS Omega 2021, 6, 17870−17879

Fangqin Cheng − *Institute of Resources and Environmental Engineering & Shanxi Collaborative Innovation Center of High Value-Added Utilization of Coal-Related Wastes, Shanxi University, Taiyuan, Shanxi 030006, China;* orcid.org/0000-0002-2961-2989; Email: cfangqin@sxu.edu.cn

Authors

Yanhong Liu − *Institute of Resources and Environmental Engineering & Shanxi Collaborative Innovation Center of High Value-Added Utilization of Coal-Related Wastes, Shanxi University, Taiyuan, Shanxi 030006, China*

Fei Wang − *Institute of Resources and Environmental Engineering & Shanxi Collaborative Innovation Center of High Value-Added Utilization of Coal-Related Wastes, Shanxi University, Taiyuan, Shanxi 030006, China*

Guangjun Lu − *Institute of Resources and Environmental Engineering & Shanxi Collaborative Innovation Center of High Value-Added Utilization of Coal-Related Wastes, Shanxi University, Taiyuan, Shanxi 030006, China*

Fengling Yang − *Institute of Resources and Environmental Engineering & Shanxi Collaborative Innovation Center of High Value-Added Utilization of Coal-Related Wastes, Shanxi University, Taiyuan, Shanxi 030006, China*

Complete contact information is available at: https://pubs.acs.org/10.1021/acsomega.1c01282

Author Contributions

Z.P. did the supervision, conceptualization, funding acquisition, methodology, project administration, validation, writing of the review, and editing. Y.L. did the data curation, methodology, and writing of the original draft. F.W. and F.C. helped in the supervision and funding acquisition. G.L. and F.Y. helped in the supervision.

Notes

The authors declare no competing financial interest.

■ ACKNOWLEDGMENTS

This work was financed by Grant-in-Aid for Scientific Research from the Major Science and Technology Projects of Shanxi Province (grant no. 20181102010) and National Natural Science Foundation of China (grant no. 21808131).

■ REFERENCES

(1) Liu, S.; Wang, S.; Xuan, S. H.; Zhang, S. S.; Fan, X.; Jiang, H.; Song, P.; Gong, X. Highly flexible multilayered e-skins for thermal-magnetic-mechanical triple sensors and intelligent grippers. *ACS Appl. Mater. Interfaces* **2020**, *12*, 15675−15685.

(2) Soltani, M.; Kulkarni, R.; Scheinost, T.; Groezinger, T.; Zimmermann, A. A. Novel approach for reliability investigation of LEDs on molded interconnect devices based on FE-analysis coupled to injection molding simulation. *IEEE Access.* **2019**, *7*, 56163−56173.

(3) Varenik, M.; Nadiv, R.; Levy, I.; Vasilyev, G.; Regev, O. Breaking through the solid/liquid process ability barrier: thermal conductivity and rheology in hybrid graphene−graphite polymer composites. *ACS Appl. Mater. Interfaces* **2017**, *9*, 7556−7564.

(4) Fox, R. J.; Yu, D.; Hegde, M.; Kumbhar, A. S.; Madsen, L. A.; Dingemans, T. J. Nanofibrillar ionic polymer composites enable high-modulus ion-conducting membranes. *ACS Appl. Mater. Interfaces* **2019**, *11*, 40551−40563.

(5) Xu, Y.; Kraemer, D.; Song, B.; Jiang, Z.; Zhou, J.; Loomis, J.; Wang, J.; Li, M.; Ghasemi, H.; Huang, X.; Li, X.; Chen, G. Nanostructured polymer films with metal-like thermal conductivity. *Nat. Commun.* **2019**, *10*, 1771.

(6) Chen, H.; Ginzburg, V. V.; Yang, J.; Yang, Y.; Liu, W.; Huang, Y.; Dua, L.; Chen, B. Thermal conductivity of polymer-based composites: fundamentals and applications. *Prog. Polym. Sci.* **2016**, *59*, 41−85.

(7) Lin, Z.; Mcnamara, A.; Liu, Y.; Moon, K. S.; Wong, C. P. Exfoliated hexagonal boron nitride-based polymer nanocomposite with enhanced thermal conductivity for electronic encapsulation. *Compos. Sci. Technol.* **2014**, *90*, 123−128.

(8) Huang, X.; Zhi, C.; Jiang, P.; Golberg, D.; Bando, Y.; Tanaka, T. Polyhedral oligosilsesquioxane-modified boron nitride nanotube based epoxy nanocomposites: an ideal dielectric material with high thermal conductivity. *Adv. Funct. Mater.* **2013**, *23*, 1824−1831.

(9) Lee, G. W.; Park, M.; Kim, J.; Lee, J. I.; Yoon, H. G. Enhanced thermal conductivity of polymer composites filled with hybrid filler. *Compos. Pt. A Appl. Sci. Manuf.* **2006**, *37*, 727−734.

(10) Yu, C.; Zhang, J.; Li, Z.; Tian, W.; Wang, L.; Luo, J.; Li, Q.; Fan, X.; Yao, Y. Enhanced through-plane thermal conductivity of boron nitride/epoxy Composites. *Compos. Pt. A Appl. Sci. Manuf.* **2017**, *98*, 25−31.

(11) Ngo, I. L.; Jeon, S.; Byon, C. Thermal conductivity of transparent and flexible polymers containing fillers: A literature review. *Int. J. Heat Mass Transfer* **2016**, *98*, 219−226.

(12) Guan, F. L.; Gui, C. X.; Zhang, H. B.; Jiang, Z. G.; Jiang, Y.; Yu, Z. Z. Enhanced thermal conductivity and satisfactory flame retardancy of epoxy/alumina composites by combination with graphene nanoplatelets and magnesium hydroxide. *Compos Part B-Eng.* **2016**, *98*, 134−140.

(13) Hu, J.; Huang, Y.; Yao, Y.; Pan, G.; Sun, J.; Zeng, X.; Sun, R.; Xu, J. B.; Song, B.; Wong, C. P. Polymer composite with improved thermal conductivity by constructing a hierarchically ordered three-dimensional interconnected network of BN. *ACS Appl. Mater. Interfaces* **2017**, *9*, 13544−13553.

(14) Moore, A. L.; Shi, L. Emerging challenges and materials for thermal management of electronics. *Mater. Today* **2014**, *17*, 163−174.

(15) Li, Q.; Chen, L.; Gadinski, M. R.; Zhang, S.; Zhang, G.; Li, H. U.; Iagodkine, E.; Haque, A.; Chen, L. Q.; Jackson, T. N.; Wang, Q. Flexible high-temperature dielectric materials from polymer nanocomposites. *Nature* **2015**, *523*, 576−579.

(16) Han, Z.; Fina, A. Thermal conductivity of carbon nanotubes and their polymer nanocomposites: a review. *Prog. Polym. Sci.* **2011**, *36*, 914−944.

(17) Miller, S. G.; Bauer, J. L.; Maryanski, M. J.; Heimann, P. J.; Barlow, J. P.; Gosau, J. M.; Allred, R. E. Characterization of epoxy functionalized graphite nanoparticles and the physical properties of epoxy matrix nanocomposites Compos. *Sci. Technol.* **2010**, *70*, 1120−1125.

(18) Changqing, L.; Mao, C.; Dongyi, Z. Effect of Filler Shape on the Thermal Conductivity of Thermal Functional Composites. *J. Nanomater.* **2017**, 1−15.

(19) Xu, X.; Chen, J.; Zhou, J.; Li, B. Thermal Conductivity of Polymers and Their Nanocomposites. *Adv. Mater.* **2018**, *30*, 1705544.

(20) Smith, D. K.; Pantoya, M. L. Effect of nanofiller shape on effective thermal conductivity of fluoropolymer composites. *Compos. Sci. Technol.* **2015**, *118*, 251−256.

(21) Wang, T.; Jiang, Y.; Huang, J.; Wang, S. High thermal conductive paraffin/calcium carbonate phase change microcapsules based composites with different carbon network. *Appl Energ.* **2018**, *218*, 184−191.

(22) Gao, Z.; Zhao, L. Effect of nano-fillers on the thermal conductivity of epoxy composites with micro-Al_2O_3 particles. *Mater Design.* **2015**, *66*, 176−182.

(23) Sanada, K.; Tada, Y.; Shindo, Y. Thermal conductivity of polymer composites with close-packed structure of nano and micro fillers. *Compos. Pt. A-Appl. Sci. Manuf.* **2009**, *40*, 724−730.

(24) Mao, L.; Han, J.; Zhao, D.; Song, N.; Shi, L.; Wang, J. Particle packing theory guided thermal conductive polymer preparation and related properties. *ACS Appl. Mater. Interfaces* **2018**, *10*, 33556−33563.

(25) Wang, S.; Cheng, Y.; Wang, R.; Sun, J.; Gao, L. Highly thermal conductive copper nanowire composites with ultralow loading: toward applications as thermal interface materials. *ACS Appl. Mater. Interfaces* **2014**, *6*, 6481−6486.
(26) Goto, T.; Ito, T.; Mayumi, K.; Maeda, R.; Shimizu, Y.; Hatakeyama, K.; Ito, K.; Hakuta, Y.; Terashima, K. Movable cross-linked elastomer with aligned carbon nanotube/nanofiber as high thermally conductive tough flexible composite. *Compos. Sci. Technol.* **2020**, *190*, 108009.
(27) Yang, R.; Chen, G.; Dresselhaus, M. S. Thermal conductivity of simple and tubular nanowire composites in the longitudinal direction. *Phys. Rev. B* **2005**, *72*, 125418.
(28) Kim, K.; Kim, J. Core-shell structured BN/PPS composite film for high thermal conductivity with low filler concentration. *Compos. Sci. Technol.* **2016**, *134*, 209−216.
(29) Feng, C. P.; Ni, H.; Chen, J.; Yang, W. Facile method to fabricate highly thermally conductive graphite/PP composite with network structures. *ACS Appl. Mater. Interfaces* **2016**, *8*, 19732−19738.
(30) Hong, H.; Jung, Y. H.; Lee, J. S.; Jeong, C.; Kim, J. U.; Lee, S.; Ryu, H.; Kim, H.; Ma, Z.; Kim, T. Anisotropic thermal conductive composite by the guided assembly of boron nitride nanosheets for flexible and stretchable electronics. *Adv. Funct. Mater.* **2019**, *29*, 1902575.
(31) Cui, X.; Ding, P.; Zhuang, N.; Shi, L.; Song, N.; Tang, S. Thermal conductive and mechanical properties of polymeric composites based on solution-exfoliated boron nitride and graphene nanosheets: a morphology-promoted synergistic effect. *ACS Appl. Mater. Interfaces* **2015**, *7*, 19068−19075.
(32) Ouyang, Y.; Hou, G.; Bai, L.; Li, B.; Yuan, F. Constructing continuous networks by branched alumina for enhanced thermal conductivity of polymer composites. *Compos. Sci. Technol.* **2018**, *165*, 307−313.
(33) Zhang, X.; Xi, X.; You, H.; Wada, T.; Chammingkwan, P.; Thakura, A.; Taniike, T. Design of continuous segregated polypropylene/Al_2O_3nanocomposites and impact of controlled Al_2O_3 distribution on thermal conductivity. *Compos. Pt. A Appl. Sci. Manuf.* **2020**, *131*, 10582.
(34) Xie, B. H.; Huang, X.; Zhang, G. J. High thermal conductive polyvinyl alcohol composites with hexagonal boron nitride micro-platelets as fillers. *Compos. Sci. Technol.* **2013**, *85*, 98−103.
(35) Xin; Zhang; Bao-Wen; Li; Lijie; Dong. Superior Energy Storage Performances of Polymer Nanocomposites via Modification of Filler/Polymer Interfaces. *Adv. Mater. Interfaces* **2018**, *5*, 1800096.
(36) Ralphs, M. I.; Kemme, N.; Vartak, P. B.; Joseph, E.; Tipnis, S.; Turnage, S.; Solanki, K. N.; Wang, R. Y.; Rykaczewski, K. In situ alloying of thermally conductive polymer composites by combining liquid and solid metal microadditives. *ACS Appl. Mater. Interfaces* **2018**, *10*, 2083−2092.
(37) Kim, K.; Kim, J. Exfoliated boron nitride nanosheet/MWCNT hybrid composite for thermal conductive material via epoxy wetting. *Compos Part B-Eng.* **2018**, *140*, 9−15.
(38) Chen, C.; Xue, Y.; Li, Z.; Wen, Y.; Li, X.; Wu, F.; Li, X.; Shi, D.; Xue, Z.; Xie, X. Construction of 3D boron nitride nanosheets/silver networks in epoxy-based composites with high thermal conductivity via in-situ sintering of silver nanoparticles. *Chem. Eng. J.* **2019**, *369*, 1150−1160.
(39) Teng, C. C.; Ma, C. C. M.; Chiou, K. C.; Lee, T. M. Synergetic effect of thermal conductive properties of epoxy composites containing functionalized multi-walled carbon nanotubes and aluminum nitride. *Compos Part B-Eng* **2012**, *43*, 265−271.
(40) He, S.; Hu, J.; Zhang, C.; Wang, J.; Chen, L.; Bian, X.; Lin, J.; Du, X. Performance improvement in nano-alumina filled silicone rubber composites by using vinyl tri-methoxysilane. *Polym. Test.* **2018**, *67*, 295−301.
(41) Yang, D.; Ni, Y.; Kong, X.; Gao, D.; Wang, Y.; Hu, T.; Zhang, L. Mussel-inspired modification of boron nitride for natural rubber composites with high thermal conductivity and low dielectric constant. *Compos. Sci. Technol* **2019**, *177*, 18−25.
(42) Pan, Z.; Wang, T.; Sun, S.; Zhao, B. Durable Microstructured Surfaces: Combining Electrical Conductivity with Superoleophobicity. *ACS Appl. Mater. Interfaces* **2016**, *8*, 1795−1804.
(43) Li, G.; Zhao, T.; Zhu, P.; He, Y.; Sun, R.; Lu, D.; Wong, C. P. Structure-property relationships between microscopic filler surface chemistry and macroscopic rheological, thermo-mechanical, and adhesive performance of SiO_2 filled nanocomposite underfills. *Compos. Pt. A-Appl. Sci. Manuf.* **2019**, *118*, 223−234.
(44) von Smoluchowski, M. *Z Phys Chem.* **1917**, *92*, 129−168.
(45) Gambinossia, F.; Mylonb, S. E.; Ferri, J. K. Aggregation kinetics and colloidal stability of functionalized nanoparticles. *Adv. Colloid Interface Sci.* **2015**, *222*, 332−349.
(46) Lin, R.; Villacorta, B.; Ge, L. Metal organic framework based mixed matrix membranes: an overview on filler/polymer interfaces. *J. Mater. Chem. A* **2018**, *6*, 293−312.
(47) Amoli, B. M.; Trinidad, J.; Rivers, G.; Sy, S.; Russo, P.; Yu, A.; Zhou, N. Y.; Zhao, B. SDS-stabilized graphene nanosheets for highly electrically conductive adhesives. *Carbon* **2015**, *91*, 188−199.
(48) Liao, Y.; Wang, Q.; Xia, H. Preparation of poly(butyl methacrylate)/γ-Al_2O_3 nanocomposites via ultrasonic irradiation. *Polym. Int.* **2001**, *50*, 207−212.
(49) Wang, X.-J.; Li, H.; Li, X. F.; Wang, Z. F.; Lin, F. Stability of TiO_2 and Al_2O_3 Nanofluids Chinese. *Phys Lett* **2011**, *28*, No. 086601.
(50) Chenjie, F.; Qiang, L.; Jibao, L.; Srikanth, M.; Qiran, C.; Xiaoliang, Z. Improving thermal conductivity of polymer composites by reducing interfacial thermal resistance between boron nitride nanotubes. *Compos. Sci. Technol.* **2018**, *165*, 322−330.

https://doi.org/10.1021/acsomega.1c01282
ACS Omega 2021, 6, 17870−17879